Scientia Iranica (2024) 31(9), 727–736

Sharif University of Technology
Scientia Iranica
Transactions C: Chemistry and Chemical Engineering
https://scientiairanica.sharif.edu

Effects of the microchannel shape upon droplet formations during synthesis of nanoparticles

F. Raji and M. Kazemeini*

Department of Chemical and Petroleum Engineering, Sharif University of Technology, Tehran, Iran.

Received 18 August 2022; received in revised form 12 February 2023; accepted 8 July 2023

KEYWORDS
Nanoparticles;
Microfluidics;
Polycaprolactone;
Microchannel;
Glass capillary device.

Abstract. Advances in nanotechnology have made it possible to produce minimal tools and equipment that can be used to control tiny volumes of fluids. Currently, at the center of attention of scientists in various fields, such systems are referred to as microfluidic systems. Also, the ability to synthesize nanoparticles with precise control over the particle's form and size is crucial. The primary goal of this research was to see if the nozzle-focused microchannels could have been used to synthesize the Polycaprolactone (PCL) polymer nanoparticles through the COMSOL Multiphysics 5.4 software medium. In this study, the velocity and static pressure of the droplet after leaving the nozzle and entering the main channel, as well as the size, shape, distribution, and weight of the droplet in terms of the time step, were understudied. It was revealed that the channel's design allowed the droplets to keep their steady structure at its conclusion. Finally, it was shown that the droplet possessed a dual functionality of place and time in terms of size and weight distribution after a time step of 0.00305 seconds. The maximum drop saturation mass was formed, and the droplet diameter size displayed a plateau after 0.01 seconds.

1. Introduction

The science of microfluidics is capable of addressing a wide range of study areas, including analysis, electronics, physics, biology, pharmaceutical sciences, etc. The attraction of microfluidics is that fluid behavior is different from the macroscale. A liquid interface may be created and broken down into droplets using various hydrodynamic techniques. These methods can be divided into three main categories: cross-flowing systems, co-flowig streams and extensional co-flows. Cross-flow systems include the collision of two fluid streams, which results in enough stress at the interface to disrupt the flow [1–3]. In co-flow systems, the stresses brought on by the adhesive forces that the external flow applies to the contact surface are what primarily leads to the formation of droplets. Finally, adjacent co-current flows where driving forces are generated by co-flowing through an orifice located in front of the internal fluid

*. *Corresponding author.*
E-mail address: kazemini@sharif.edu (M. Kazemeini)

To cite this article:
F. Raji and M. Kazemeini "Effects of the microchannel shape upon droplet formations during synthesis of nanoparticles", *Scientia Iranica* (2024), **31**(9), pp. 727-736
DOI: 10.24200/sci.2023.60984.7089

source. To get a liquid droplet or droplets, this induces pressure gradients or dilatational viscous stresses that pull the interface [4].

According to published reports, polymers have found many applications in treatment programs due to the variety of different operating methods, various methods of macromolecular synthesis, and their chemical and physical diversities. In this direction, polymer nanoparticles improve and facilitate modern medicine and nanomedicine [5]. The scientific community in recent decades has considered biodegradable polymer nanoparticles due to their high potential for drug delivery. Solvent emulsion evaporation, desalination, dialysis, nano-deposition, and supercritical fluid technology may all be used to make polymer nanoparticles from pre-prepared polymers. Polymerization processes such as microemulsion, mini-emulsion, emulsion without surfactant, and intermediate polymerization can also synthesize them directly from monomers [6–8]. Due to the possibility of high control over the synthesis process, microchannels achieve essential features that other synthesis methods do not have. Such as achieving a uniform particle size distribution and the relative ease of controlling particle size by changing the effective parameters in the particle synthesis process [9–16]. In synthesizing materials by microchannels (such as similar processes such as energy production or extraction of biomolecules, ions, and dyes), there are three main influential parameters: flow patterns, residence time, and mixing length [17–21]. Zhang et al [22]. used a microfluidic synthesis system to present Gas/Liquid/Liquid (G/L/L) emulsion droplets with various configurations and observed the deformation from the shell core structure to Janus droplets. The results reveal that the equilibrium angle influences the shape of the G/L/L emulsion at the contact line and the relative volume of the two dispersed phases. Setting relative velocity, continuous phase viscosity, surface tension, and type and concentration of surfactants allows for creation of Janus droplets with various morphologies. Bariki et al. [23]. produced polycaprolactone nanoparticles in a co-flow glass capillary device with a tip size of 250 μm. They simulated the droplet formation process in the co-flow microchannel using Computational Fluid Dynamics (CFD). The results show that the ratio of microdroplets to nanoparticles was between 735 and 75. In another study of this group [24], The formation of core/shell microdroplets with uniform size has been investigated numerically in a co-flow microchannel. Finally, they proposed a correlation for the shell thickness using the shell-to-core phase velocity ratio and performed 51 CFD simulations. Using a co-flow microfluidic device, Zhang et al. [25] prepared a magnetic chitosan microsphere without using any surfactant or cross-linking agent. This method creates magnetic chitosan microspheres of even-sized. Another study [26] suggests a straightforward, droplet-based technique for producing polymer microspheres without surfactants. The findings indicate that the critical determinants of the microspheres' properties are the surface tension between the polymer solution and the continuous phase, the water flow pattern in the continuous phase, and the viscosity of the solvent for the polymer solution. To manufacture Janus particles made of poly (D-lactic acid) (PLA) and poly (C-lactic acid) (PCL), Ekanem et al. [27] developed a concentrated flow capillary microfluidic synthesis platform. A concentrated reverse flow or a contemporaneous flow paired with a concentrated reverse flow was used to create large droplets. Janus nanoparticles were then produced by mixing two separate polymer streams in two parts. Lince et al. [28] PCL nanoparticles were created in a Confined Impinging Jets Reactor (CIJR), and it was found that mixing had a significant impact on the final particle size. The mixing efficiency improves by increasing the flow rate of liquid phases into the CIJR. This increase led to favorable nucleation and a significant reduction in particle size. Nanoparticles with regulated size, adhesion qualities, and controlled degradation must be created to achieve controlled drug secretion to a specific spot at the required therapeutic rate [29]. Due to their relatively high capacity, traditional mixers need more refined control over the mixing process, resulting in poor particle size distribution control. Agitators or micro-scale reactors have a minimal volume of liquids, allowing a homogeneous reaction medium to be achieved and having a higher surface-to-volume ratio than conventional agitators [30]. Ali et al. [31] prepared hydrocortisone nanoparticles in a Y-junction microfluid. The flow rate of the solvent and anti-solvent influenced the size of the nanoparticles formed, with smaller particles forming at higher flow rates. Su et al. [32] prepared Barium Sulfate and 2,2-Dipyridylamine nanoparticles using a microfluidic system through T-shaped tubes. Droplets of solvent and anti-solvent materials were thus gathered downstream of the T-shaped channel after forming at its entrance. Génot et al. [33]. Used a Y-shaped microchannel, a 3D focusing hydrodynamic device, to synthesize Rubrene nanocrystals through the non-solvent crystallization process. Othman et al. [34] biodegradable polymer nanoparticles were created inside a rectangular tube with an internal diameter of 1 mm. They used a micromixer combined with nano-deposition in a glass-capillary device. Water and organic phase micromixtures (1% by weight of polylactic or polycaprolactone) dissolved in Tetrahydrofuran (THF) were modeled using the COMSOL Multiphysics software. Nanoparticle Tracking Analysis (NTA), dynamic light scattering, and in situ microscopic imaging were also used to investigate it in vitro. Numerical results

matched experimental observations in terms of flow patterns and mean particle size. Xie et al. [35] developed a fluid nano-deposition system that produced a single-step encapsulates paclitaxel hydrochloride and doxorubicin (hydrophobic and hydrophilic medicines, respectively) in Janus polymer nanoparticles made of poly (lactic-co-glycolic acid) (PLGA). Lone et al. came up with yet another model. It is a T-shaped microchip that synthesizes Janus particles by isolating the downstream channel's ultra violet phase [36]. PCL polymer nanoparticles with suitable biocompatibility and biodegradability properties are one of the best options for application in drug delivery processes. Precise control over the size and shape of the nanoparticles is critical during their synthesis [37]. The primary purpose of this research was to synthesize PCL nanoparticles using a microchannel focused on nozzle flow through the COMSOL software. The device's primary body is made up of two coaxial glass capillaries, one having a circular cross-section and the other with a circular cross-section but a nozzle form. The continuous phase was located at the main channel, and the dispersed phase was injected with a nozzle. It is reiterated that, due to the extended run-time of the simulation, only the formation of one drop was investigated.

2. Theory

Biphasic fluids occur in natural problems and have many applications in industrial problems. One of the most critical problems in the two-phase modeling of fluids is how to model the surface tension at its correct location as a force or stress. This is because surface tension is a force of discontinuous nature that makes it difficult to model this type of currency. Dispersed and continuous-phase fluids typically enter the device through two independent microchannels in two-phase microfluidic devices. Depending on the geometry of the microfluidic device, the channels are usually positioned at a junction. The junction shape aids in defining local flow fields that depict the deformation of the two-fluid interface. The free surface instability between the phases must be significant enough for the droplets to develop and finally split from the scattered phase. The conflict between the stabilizing and destabilizing forces in the two interfacial phases causes instability. For steady currents, droplet formation in microchannels is usually intermittent and integrated in order to generate a jet; free surface instabilities must be kept to a minimum. Shear stresses and fluid immobility are joint stabilizing factors that create jets. Also, capillary pressure is frequently the leading cause of joint instability and droplet formation.

Various geometries, including flow-focused, have been used to produce polymer nanoparticles. For example, nanoparticle synthesis will be challenging if the flow geometry of the orifice diameter is too large or too small. Therefore, the type of microchannel geometry is essential in synthesizing nanoparticles and all processes. The microchannels studied in this study, as shown in Figure 1, are formed by punctuation and passing a line through them. Due to this geometry possessing an axial symmetry, the developed model also reduced the computational cost.

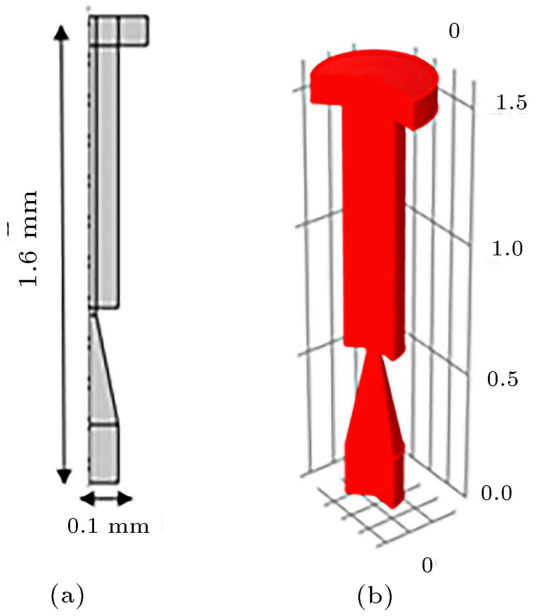

Figure 1. (a) Desired microchannel geometry developed through the COMSOL software in this research and (b) A three-dimensional view of the generated microchannel of part (a) to form the PCL droplets.

Biphasic fluid modeling methods can be divided into two general types, Lagrangian and Eulerian. Lagrangian methods have disadvantages such as high computational cost, and also, if the mesh is used, the shape of the elements becomes unsuitable over time. On thte other hands, the Eulerian methods are more popular due to their lower computational cost. One of the essential Eulerian methods is the fluid's surface method and volume fraction. Amongst the most important Eulerian methods one may utilize is the Level set method and Volume of Fluid (VOF). The continuity equation for an incompressible flow is given by the following relation:

$$\nabla.u = 0. \tag{1}$$

The incompressible Navier-Stokes Eq. (2), coupled with the Level Set equation (which is explained in detail below) is provided as follows:

$$\rho\frac{Du}{Dt} = -\nabla P + \rho g + \mu\nabla^2 u + F_S. \tag{2}$$

The Level Set equation was first introduced in 1988 to model multiphase incompressible fluids [38]. One of

the major problems of this method is the loss of mass during calculations. In such method, a signed distance function is defined, and the basic idea is to consider a continuous scalar function called φ. The boundary between two fluids is known as the function φ equals to zero. Here, for $\varphi < 0$ one side of the boundary is considered while for $\varphi > 0$ the other side of such boundary may be undertaken. At the beginning of the solution, the Level Set function is defined as the minimum signed distance function to the level (i.e.; the boundary). Therefore, in the solution region, $|\nabla\varphi| = 1$. When the boundary is advanced by an external velocity field, the behavior of the Level Set function due to the movement of the boundary is calculated by the following displacement equation:

$$\frac{\partial\varphi}{\partial t} + u.\nabla\varphi = 0, \tag{3}$$

where t represents time, and u is the velocity field. This displacement equation is solved locally near the boundary. If the fluid flow is incompressible hence, $\nabla u = 0$ and the displacement equation shall be written as:

$$\frac{\partial\varphi}{\partial t} + \nabla.(u\varphi) = 0. \tag{4}$$

Eq. (2) corresponds to the continuity equation for the Level Set function. This function is positive in one phase and negative in the other. In both phases, a step function is used to represent the density and viscosity of fluids such that;

$$H(\varphi) = \begin{cases} 0, & \varphi < 0 \\ 1, & \varphi > 0 \end{cases} \tag{5}$$

The Level Set function is defined as a signed distance function concerning the border, i.e.:

$$|\varphi(X)| = d(X) = \min(|X - X_1|), \qquad X_1 \in I, \tag{6}$$

where I represents the border and X displays the distance.

In numerical simulations, the step function has discontinuity points. At that value, the function suddenly changes from one value to another, which causes instability in numerical simulation using the finite element method. To overcome this problem, the following function is used instead of the previous one:

$$H_{sm}(\varphi) = \begin{matrix} 0 \\ \{\frac{1}{2} + \frac{\varphi}{2\varepsilon} + \frac{1}{2\Pi}\sin(\frac{\Pi\varphi}{\varepsilon}) \\ 1 \end{matrix} \quad \begin{matrix} \varphi < -\varepsilon \\ -\varepsilon \le \varphi \le \varepsilon \\ \varphi > \varepsilon \end{matrix} \tag{7}$$

where ε represents half the thickness of the border. As a result, the new Level Set function possesses the form of Eq. (8):

$$\tilde{\varphi}(x,t) = H_{sm}(\varphi(x,t)). \tag{8}$$

According to the φ function, the curvature of the boundary may be calculated with high accuracy. Although there is some mass loss in the mentioned method, these minor errors become of large values as time goes by. To overcome this problem, on 2005, a Conservative Level Set method that has high accuracy and good mass survival [39] was developed. In the current study, this latter method is used to investigate the behavior of the boundary between two fluids. Through the Level Set function in this method, the border is shown with a value of 0.5, the continuous phase fluid with a value of 0 and the drop forming phase fluid with a value of 1. This method calculates the density and viscosity along the border by Eqs. (9) and (10):

$$\rho(x,t) = \rho_c + (\rho_c - \rho_d)\varphi, \tag{9}$$

$$\mu(x,t) = \mu_c + (\mu_c - \mu_d)\varphi, \tag{10}$$

where the ρ_c and ρ_d are the density of continuous and dispersed phases; respectively, and μ_c and μ_d are the viscosities of these two phases. In two-phase fluid simulation, boundary normal vector and boundary curvature are the two values required to model the surface tension, which is calculated by Eqs. (11) and (12) as follows:

$$\hat{n} = \frac{\nabla\varphi}{|\nabla\varphi|}, \tag{11}$$

$$k = \nabla.\frac{\nabla\varphi}{|\nabla\varphi|}, \tag{12}$$

where $\hat{n}$ is the vector normal to the boundary and k is the local curvature of the boundary.

The equations utilized in this section are as follows. It should be noted that, Eq. (13) is totally compatible with those of the software's literature [40–46]. Equations for two-phase surface regulation and fluid volume fraction:

$$\frac{\partial\Phi}{\partial t} + u.\nabla\Phi = \gamma\nabla.\left(\varepsilon_{ls}\nabla\Phi - \Phi(1-\Phi)\frac{\nabla\Phi}{|\nabla\Phi|}\right),$$
$$\Phi = Phils. \tag{13}$$

In Eq. (13), γ and ε are the stabilizing parameters of the numerical solution. γ is the restart parameter, its value is determined according to the highest fluid velocity in the system, and ε is the boundary thickness parameter determined according to the mesh size of the system. The boundary conditions utilized in the present model are provided through Table S.1 in the Supplementary data.

3. Solution method

One of the essential aspects of all numerical analysis research is how to create a network or mesh the

problem. In this venue, the size of the selected network to numerically solve the problem directly affects the results. To form droplets in nanometer dimensions, a tiny network size must be developed at the center of the microchannel (i.e., the connection joint of the microchannels). More extensive networks may be used in the rest of the microchannel areas to optimize while minimizing the solution time. To solve this problem, a Quad/Tri mesh was used. It is better to use very small meshes only at two-phase regions to achieve less computational time.

The networking should be determined such that the simulation results are independent of the shape and size of the networks; hence, they do not affect the results. Therefore, after completing the model, one has to perform a network independence test to ensure the results' accuracy. In order to investigate the network size, it is important to remember that the smaller the network, the greater the accuracy of the calculations; however; this also increases the computing cost. Therefore, it is necessary to find an optimal value for networking the microchannel area, the reduction of which has minimal effect on the results. An example of a networking independence diagram is provided in Figure 2, displaying the mesh element utilized in this study.

The Mesh statistics generated by the COMSOL software are also tabulated in Table 1 to provide a more complete depiction of the aforementioned networking towards emphasizing the accuracy of this model.

According to some research works reported in the open literature, the electric potential was employed for the mesh independence test [18,47–50]. However; In the present study, an electric potential was not applied in accordance with some other published works, instead fluid flow based upon velocity as a result was utilized. This is determined using Eq. (5). The value $U_{initial}$ was chosen based upon the nozzle inlet diameter. Figure 3 demonstrates that its value is nearly constant starting at 5×10^4. Then, to perform the mesh independency's investigations, a dimensionless velocity was defined ass follows:

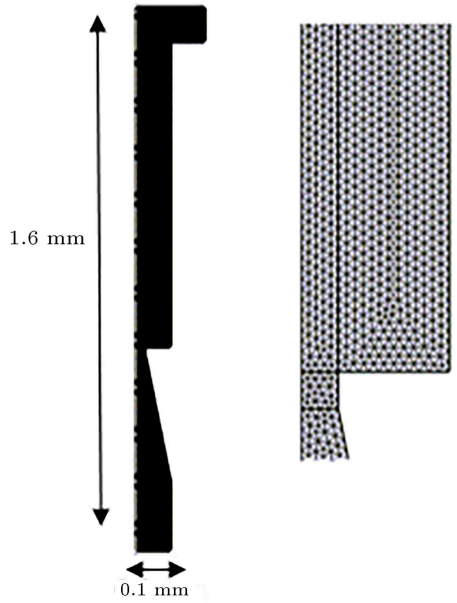

Figure 2. The mesh configuration developed in the present study based upon the COMSOL software simulation.

Table 1. Mesh statistics generated through the COMSOL software.

Mesh statistics	
Description	**Value**
Minimum element quality	0.7435
Average element quality	0.9734
Triangle	8444
Edge element	731
Vertex element	17

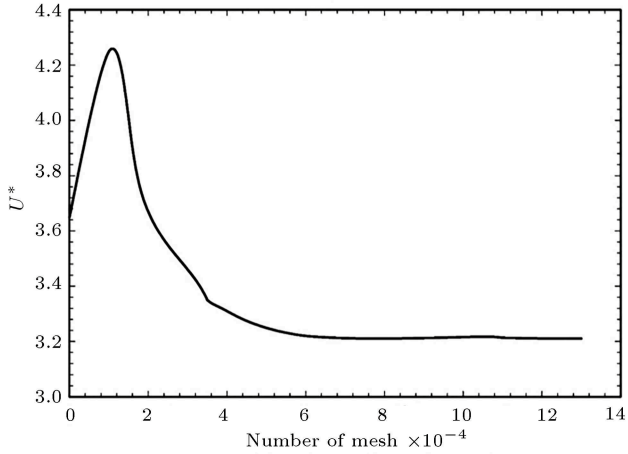

Figure 3. Variations of the dimensionless velocity U^* as a function of number of meshes towards checking the mesh independency.

$$U^* = \frac{U}{U_{initial}}, \tag{14}$$

where the onset of U^* leveling off is indicative of the threshold of having reached mesh independent calculations.

A systematic flowchart (i.e.; a process flow diagram) for calculations performed in this research is provided through Figure S.1 in the Supplementary data of this paper.

Moreover, the present simulation data was validated with the simulation results of Li et al. [51]. For this purpose, the pressure distribution in the microchannel section was determined and according to Figure 4, a very satisfying comparison was established between the data generated through the present work and that of Li et al. This emphasized correct operation

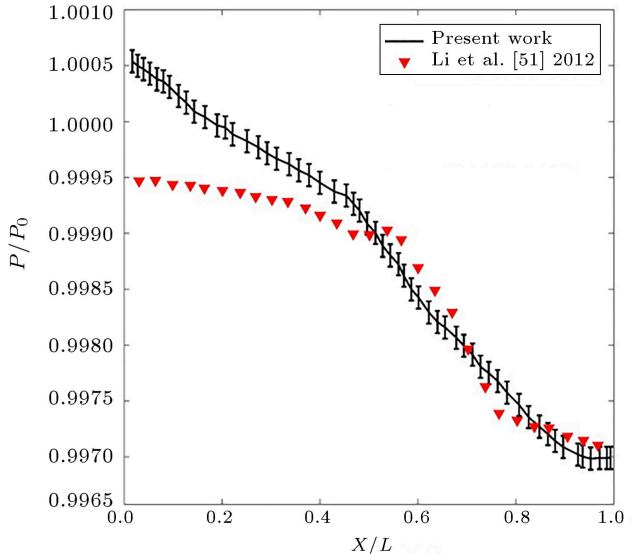

Figure 4. Variations of the reduced pressure through the dimensionless reactor length. A comparison between simulated data obtained from the present model with those of Li et al. [51]. Vertical lines represent the error bars for which a min and max values of 0.005% and 0.064%, respectively are determined through formulae provided in Eqs. of S.1 and S.2 in Supplementary data of this paper.

of the model using two phase flow equations was followed. It is reiterated that, since the onset of the study by Li et al. [51] started at the 20% of the reactor length, the simulation results of the present work also started at that position onwards.

4. Results and discussion

This section presents the results of a numerical study of the production process of the PCL polymer nanoparticles using a nozzle-focused microchannel in COMSOL Multiphysics 5.4. software medium is performed. Ultimately, through this, one can better understand what goes through synthesizing such materials, which may later be used to optimize the involved process. The microchannel under study is a nozzle microchannel, the 3D view of which is shown in Figure 1(b). In this microchannel, the phenomenon of mass transfer and hydrodynamics of droplets has been investigated. Parameters such as the droplet size (in particular, its diameter), droplet weight, flow velocity effect, and fluid pressure were also investigated, which shall be discussed shortly.

Figure 5 displays the velocity contour and static pressure of the droplet after leaving the nozzle and entering the main channel. As shown in Figure 6(a), the static pressure at the beginning of the channel increases due to the change in the cross-sectional area at the inlet. However, the amount of total pressure is constant throughout the channel and due to the boundary condition imposed, the pressure will increase

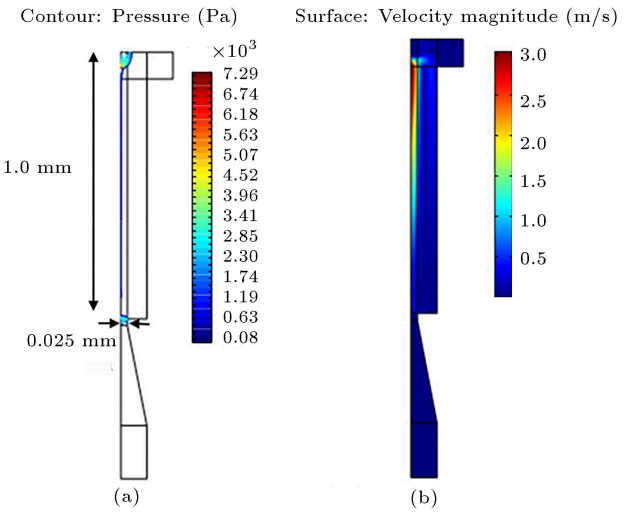

Figure 5. (a) pressure contour and (b) fluid velocity contour for the generated droplet through the COMSOL software in the present research.

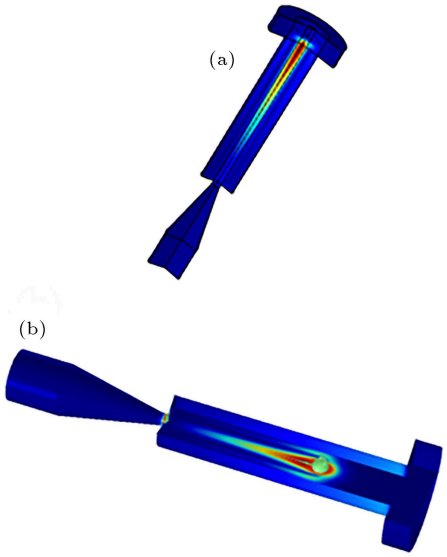

Figure 6. (a) The 3D fluid velocity contour and (b) the 3D contour of droplets developed into the microchannel which were generated through the COMSOL software in the present research.

again at the end of the channel. As a result, the beginning and endpoint of the channel will have the most significant impacts upon the droplet formation due to the end effects. On the other hand, through the Figure 6(b), the velocity profile emphasizes that, at the beginning of the droplet entering the channel, a path called the *Developed Length* is followed to reach the maximum velocity in the laminar flow region. In addition, due to the micron scale of the channel and the compressive driving force, the velocity profile tends towards that of the plug flow. Moreover, due to the micron scale of the channel and the pressure driving force, the velocity profile is inclined towards the plug behavior. In addition, except upon the walls,

the average maximum velocity is observed across the channel. Therefore, at the end of 1/3 of the channel, at a constant maximum velocity, the droplets maintain their stable shapes.

From another point of view, Figure 6 shows the fluid velocity contour and droplet formation in athree-dimensional aspect. As mentioned in Figure 5, the threshold is the beginning of the developed zone and helps forming a stable droplet shape at the end of the channel.

Next, in Figure 6(a), the fluid velocity around the droplet represents the flow lines which may indicate the degree of distortion and deviation in the droplet formation path. Nonetheless, one is cautioned that, this flow area being considered is that of the fully developed one through which a maximum velocity is reached and the system is still within the laminar flow regime. Yet, Figure 6(b) displays the motion of a drop in the bulk of the fluid. This figure clearly reveals dead zones exist around a given drop. Therefore, in order to control the droplet size, in addition to the microchannel width, the droplet size distribution may be controlled by balancing the Lift and Drag forces. As can be seen from this figure, if the Lift force overcomes that of the Drag, the shape of the drop will change from spherical to oval. In general, it is a foregone conclusion that, the velocity profile in both 2 and 3D views have significant effects upon determining the shape, size, and distribution of droplets.

Figure 7 shows the changes in droplet weight and size distribution over time. As discussed in the velocity profile, the stability of the droplet in terms of size, shape, distribution, and weight is a function of the path taken along the microchannel to enter the fully developed regions. In addition to the locality dimension, this also requires a time dimension due to the continuity of the process. In Figure 7(b), at the beginning of the process, when the droplet enters the main channel from the nozzle tank, it gathers molecules around it to make the final shape. According to the balance between the interfacial forces and the contact angle, the adjacent fluid flow rate also possesses a saturation point of weight gain. According to Figure 7(b), after a time step of 0.003 seconds, the maximum drop saturation mass is formed. After this period of time, as mentioned before, the balance of body forces due to entering the fully developed region displays a uniform behavior, and the weight of the drop remains almost constant. From another point of view, Figure 7(a) reveals the particle size distribution of droplets at different time intervals.

As mentioned in Figure 6(b), due to the sizes of the Lift and Drag forces, the probability of deformation of the droplet diameter at the initial time steps is rather high. Nonetheless, upon reaching the fully developed region and then after, these changes remain almost constant.

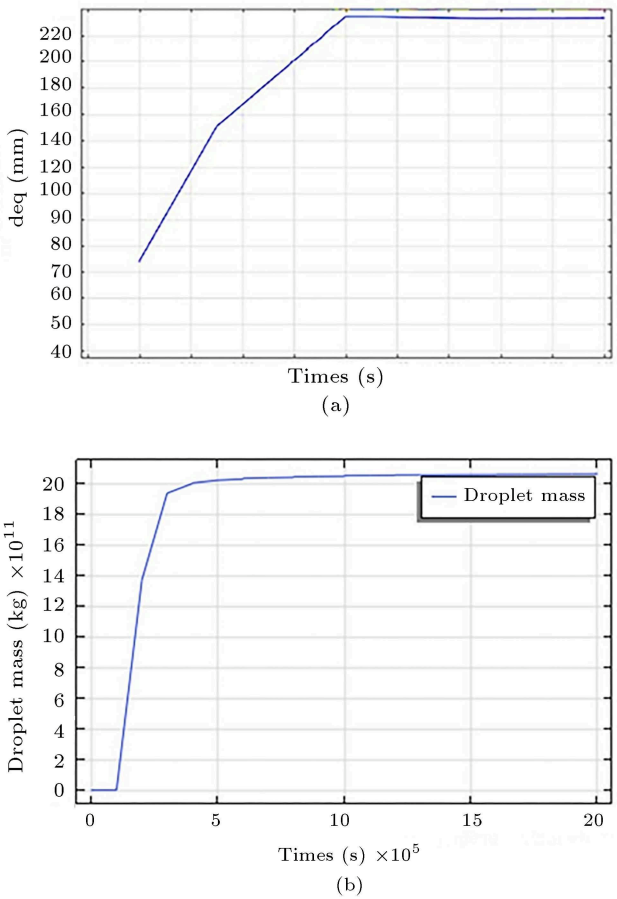

Figure 7. specifications of the generated droplet as a function of time elapsed after detachment from the microchannel (a) the size and (b) the weight of the droplets formed.

In general, it can be concluded from Figure 7 that the droplets have a locality and time function in size and weight distribution. Therefore, a specific size distribution can be easily achieved by controlling two parameters, including channel length and process time. One observes that the drop weight stabilizes at 0.00305 seconds, and the drop diameter is fixed after 0.01 seconds.

5. Conclusions

This contribution examined the possibility of synthesizing polycaprolactone nanoparticles utilizing nozzle-focused microchannels through the COMSOL Multiphysics 5.4 software. The Eulerian method was used because of its many advantages in particular; the cost effectiveness over the Lagrangian method. The primary body of the device under investigation is made up of two coaxial glass capillaries, one having a circular cross-section and one with a circular cross-section but a nozzle form. The continuous phase flows in the main channel and the scattered phase within the nozzle. Due to the droplet's static pressure, the channel's beginning

and endpoints had the most significant effect upon the droplet formation due to the end effect. The velocity profile also confirmed this. Moreover, the velocity profile tended toward that of the plug flow. In addition to the microchannel width, the balance of Lift and Drag forces was used to control the droplet size. With the Lift force prevailing over the Drag, the droplet shape changed from spherical to oval, indicating that the velocity profile was influential in determining the distribution size and shape of the droplets. These indeed were revealed to be a function of reaching (i.e.; of locality) toward the fully developed region. They also required a time dimension to do so. According to the balance of surface forces, the contact angle, and the flow rate of the fluid adjacent to the droplet, with a time step of 0.003 seconds, the maximum saturation mass of the droplet was formed. After that, it behaved uniformly, and the drop's weight remains almost constant.

An outlook of the present study could lay a good background for a better understanding of how to determine such liquid material physical properties as surface and/or interfacial tensions. However, more experimental undertakings are in order.

Supplementary data

Supplementary data is available at:
file:///C:/Users/SHAMILA/Downloads/Supplementary%20data%20Last-1.pdf

References

1. Elvira, K.S., Gielen, F., Tsai, S.S.H., et al. "Materials and methods for droplet microfluidic device fabrication", *Lab Chip*, **22**(5), pp. 859–875 (2022). https://doi.org/10.1039/D1LC00836F
2. Paramanantham, S.S.S., Nagulapati, V.M., and Lim, H. "Numerical investigation of the influence of microchannel geometry on the droplet generation process", *Journal of Applied Fluid Mechanics*, **15**(5), pp. 1291–1305 (2022). https://doi.org/10.47176/JAFM.15.05.1126
3. Roshchin, D.E. and Patlazhan, S.A. "Mixing inside droplet co-flowing with Newtonian and shear-thinning fluids in microchannel", *International Journal of Multiphase Flow*, **158**, p. 104288 (2023). https://doi.org/10.1016/j.ijmultiphaseflow.2022.104288
4. Mathies, R.A. and Huang, X.C. "Capillary array electrophoresis: an approach to high-speed, high-throughput DNA sequencing", *Nature*, **359**(6391), pp. 167–169 (1992). https://doi.org/10.1038/359167a0
5. Banik, B.L., Fattahi, P., and Brown, J.L. "Polymeric nanoparticles: the future of nanomedicine", *WIREs Nanomedicine and Nanobiotechnology*, **8**(2), pp. 271–299 (2016). https://doi.org/10.1002/wnan.1364
6. Yadav, H.K. "Different techniques for preparation pf polymeric nanoparticles-A", *Asian Journal of Pharmaceutical and Clinical Research*, **5**(3), pp. 16–23 (2012). https://doi.org/10.1214/j.ajpcr.2012.0974-2441
7. Rao, J.P. and Geckeler, K.E. "Polymer nanoparticles: Preparation techniques and size-control parameters", *Prog Polym Sci*, **36**(7), pp. 887–913 (2011). https://doi.org/10.1016/j.progpolymsci.2011.01.001
8. Galindo-Rodriguez, S., Allémann, E., Fessi, H., et al. "Physicochemical parameters associated with nanoparticle formation in the salting-out, emulsification-diffusion, and nanoprecipitation methods", *Pharm Res*, **21**(8), pp. 1428–1439 (2004). https://doi.org/10.1023/B:PHAM.0000036917.75634.be
9. Jahn, A., Vreeland, W.N., DeVoe, D.L., et al. "Microfluidic directed formation of liposomes of controlled size", *Langmuir*, **23**(11), pp. 6289–6293 (2007). https://doi.org/10.1021/la070051a
10. Stone, H.A., Stroock, A.D., and Ajdari, A. "Engineering flows in small devices: Microfluidics toward a lab-on-a-chip", *Annu Rev Fluid Mech,* **36**(1), pp. 381–411 (2004). https://doi.org/10.1146/annurev.fluid.36.050802.122124
11. Koh, C.G., Zhang, X., Liu, S., et al. "Delivery of antisense oligodeoxyribonucleotide lipopolyplex nanoparticles assembled by microfluidic hydrodynamic focusing", *J Control Release*, **141**(1), pp. 62–69 (2010). https://doi.org/10.1016/j.jconrel.2009.08.019
12. Belliveau, N.M., Huft, J., Lin, P.J., et al. "Microfluidic synthesis of highly potent limit-size lipid nanoparticles for in vivo delivery of siRNA", *Mol Ther Nucleic Acids*, **1**(8), p. e37 (2012). https://doi.org/10.1038/mtna.2012.28
13. Chen, S., Zhang, H., Shi, X., et al. "Microfluidic generation of chitosan/CpG oligodeoxynucleotide nanoparticles with enhanced cellular uptake and immunostimulatory properties", *Lab Chip*, **14**(11), pp. 1842–1849 (2014). https://doi.org/10.1039/C4LC00015C
14. Karnik, R., Gu, F., Basto, P., et al. "Microfluidic platform for controlled synthesis of polymeric nanoparticles", *Nano Lett*, **8**(9), pp. 2906–2912 (2008). https://doi.org/10.1021/nl801736q
15. Kolishetti, N., Dhar, S., Valencia, P.M., et al. "Engineering of self-assembled nanoparticle platform for precisely controlled combination drug therapy", *Proceedings of the National Academy of Sciences*, **107**(42), pp. 17939–17944 (2010). https://doi.org/10.1073/pnas.1011368107
16. Valencia, P.M., Basto, P.A., Zhang, L., et al. "Single-step assembly of homogenous lipid-polymeric and lipid-quantum dot nanoparticles enabled by microflu-

idic rapid mixing", *ACS Nano*, **4**(3), pp. 1671–1679 (2010).
https://doi.org/10.1021/nn901433u

17. Raji, F. and Rahbar-Kelishami, A. "Evaluation of biocompatible aqueous two-phase systems with the double interface for the recovery of biomolecules", *Colloids Surf A Physicochem Eng Asp*, **624**(May), 126823 (2021).
https://doi.org/10.1016/j.colsurfa.2021.126823

18. Khatibi, M., Ashrafizadeh, S.N., and Sadeghi, A. "Augmentation of the reverse electrodialysis power generation in soft nanochannels via tailoring the soft layer properties", *Electrochim Acta*, **395**, p. 139221 (2021).
https://doi.org/10.1016/j.electacta.2021.139221

19. Raji, F. and Rahbar-kelishami, A. "Chemical engineering and processing - process intensification evaluation of mass transfer rate in aqueous two-phase systems: Effect of microchannel width for bovine serum albumin extraction", *Chemical Engineering and Processing - Process Intensification*, **163**(February), p. 108370 (2021).
https://doi.org/10.1016/j.cep.2021.108370

20. Khatibi, M., Sadeghi, A., and Ashrafizadeh, S.N. "Tripling the reverse electrodialysis power generation in conical nanochannels utilizing soft surfaces", *Physical Chemistry Chemical Physics*, **23**(3), pp. 2211–2221 (2021).
https://doi.org/10.1039/D0CP05974A

21. Raji, F., Shayesteh, H., and Rahbar-Kelishami, A. "Y-Y microfluidic polymer/salt aqueous two-phase system for optimization of dye extraction: Evaluation of channel geometry", *Separation Science and Technology*, (Philadelphia), **57**(15), pp. 2471–2481 (2022).
https://doi.org/10.1080/01496395.2022.2059677

22. Zhang, S.-B., Ge, X.-H., Geng, Y.-H., et al. "From core-shell to Janus: Microfluidic preparation and morphology transition of gas/oil/water emulsions", *Chem Eng Sci*, **172**, pp. 100–106 (2017).
https://doi.org/10.1016/j.ces.2017.06.031

23. Ghasemzade Bariki, S., Salman, M., and Ghojavand, M. "Computational fluid dynamic study of polycaprolactone nanoparticles precipitation in a co-flow capillary micro-tube", *Canadian Journal of Chemical Engineering*, **101**(8), pp. 4746–4761 (2022).
https://doi.org/10.1002/cjce.24768

24. Bariki, S.G. and Movahedirad, S. "A flow map for core/shell microdroplet formation in the co-flow Microchannel using ternary phase-field numerical model", *Sci Rep*, **12**(1), p. 22010 (2022).
https://doi.org/10.1038/s41598-022-26648-3

25. Zhang, Y., Wang, D., Bai, X., et al. "Microfluidic preparation of magnetic chitosan microsphere and its adsorption towards Congo red", *Journal of Polymer Research*, **30**(2), p. 77 (2023).
https://doi.org/10.1007/s10965-022-03387-7

26. Zhang, Y., Wang, Y., Du, G., et al. "A surfactant-free droplet based microfluidic technique for the fabrication of polymeric microspheres", *Mater Today Commun*, **33**, p. 104389 (2022).
https://doi.org/10.1016/j.mtcomm.2022.104389

27. Ekanem, E.E., Zhang, Z., and Vladisavljević, G.T. "Facile production of biodegradable bipolymer patchy and patchy janus particles with controlled morphology by microfluidic routes", *Langmuir*, **33**(34), pp. 8476–8482 (2017).
https://doi.org/10.1021/acs.langmuir.7b02506

28. Lince, F., Marchisio, D.L., and Barresi, A.A. "Strategies to control the particle size distribution of poly-ε-caprolactone nanoparticles for pharmaceutical applications", *J Colloid Interface Sci*, **322**(2), pp. 505–515 (2008).
https://doi.org/10.1016/j.jcis.2008.03.033

29. Mohanraj, V.J. and Chen, Y. "Nanoparticles - a review", *Tropical Journal of Pharmaceutical Research*, **5**(1), pp. 561–573 (2007).
https://doi.org/10.4314/tjpr.v5i1.14634

30. Capretto, L., Carugo, D., Mazzitelli, S., et al. "Microfluidic and lab-on-a-chip preparation routes for organic nanoparticles and vesicular systems for nanomedicine applications", *Adv Drug Deliv Rev*, **65**(11–12), pp. 1496–1532 (2013).
https://doi.org/10.4314/tjpr.v5i1.14634

31. Ali, H.S.M., York, P., and Blagden, N. "Preparation of hydrocortisone nanosuspension through a bottom-up nanoprecipitation technique using microfluidic reactors", *Int J Pharm*, **375**(1–2), pp. 107–113 (2009).
https://doi.org/10.1016/j.ijpharm.2009.03.029

32. Su, Y.Ã., Kim, H., Kovenklioglu, S., et al. "Continuous nanoparticle production by microfluidic-based emulsion, mixing and crystallization", **180**, pp. 2625–2629 (2007).
https://doi.org/10.1016/j.jssc.2007.06.033

33. Génot, V., Desportes, S., Croushore, C., et al. "Synthesis of organic nanoparticles in a 3D flow focusing microreactor", *Chemical Engineering Journal*, **161**(1–2), pp. 234–239 (2010).
https://doi.org/10.1016/j.cej.2010.04.029

34. Othman, R., Vladisavljević, G.T., Bandulasena, H.C.H., et al. "Production of polymeric nanoparticles by micromixing in a co-flow microfluidic glass capillary device", *Chem. Eng. J.*, **280**, p. 316 (2015).
https://doi.org/10.1016/j.cej.2015.05.083

35. Xie, H., She, Z.-G., Wang, S., et al. "One-step fabrication of polymeric Janus nanoparticles for drug delivery", *Langmuir*, **28**(9), pp. 4459–4463 (2012).
https://doi.org/10.1021/la2042185

36. Lone, S., Kim, S.H., Nam, S.W., et al. "Microfluidic synthesis of Janus particles by UV-directed phase separation", *Chem. Commun.*, **47**(9), pp. 2634–2636 (2011).
https://doi.org/10.1039/C0CC04517A

37. Heshmatnezhad, F. and Solaimany Nazar, A.R. "On-chip controlled synthesis of polycaprolactone nanoparticles using continuous-flow microfluidic devices", *J*

Flow Chem, **10**(3), pp. 533–543 (2020). https://doi.org/10.1007/s41981-020-00092-8

38. Osher, S. and Sethian, J.A. "Fronts propagating with curvature-dependent speed: Algorithms based on Hamilton-Jacobi formulations", *J Comput Phys*, **79**(1), pp. 12–49 (1988). https://doi.org/10.1016/0021-9991(88)90002-2
39. Bashir, S., Rees, J.M., and Zimmerman, W.B. "Investigation of pressure profile evolution during confined microdroplet formation using a two-phase level set method", *International Journal of Multiphase Flow*, **60**, pp. 40–49 (2014). https://doi.org/10.1016/j.ijmultiphaseflow.2013.11.012
40. Khatibi, M., Ashrafizadeh, S.N., and Sadeghi, A. "Covering the conical nanochannels with dense polyelectrolyte layers significantly improves the ionic current rectification", *Anal Chim Acta*, **1122**, pp. 48–60 (2020). https://doi.org/10.1016/j.aca.2020.05.011
41. Seifollahi, Z. and Ashrafizadeh, S.N. "Effect of charge density distribution of polyelectrolyte layer on electroosmotic flow and ion selectivity in a conical soft nanochannel", *Chem Eng Sci*, **261**, p. 117986 (2022). https://doi.org/10.1016/j.ces.2022.117986
42. Seifollahi, Z. and Ashrafizadeh, S.N. "Ionic-size dependent electroosmotic flow in ion-selective biomimetic nanochannels", *Colloids Surf B Biointerfaces*, **216**, p. 112545 (2022). https://doi.org/10.1016/j.colsurfb.2022.112545
43. Dartoomi, H., Khatibi, M., and Ashrafizadeh, S.N. "Enhanced ionic current rectification through innovative integration of polyelectrolyte bilayers and charged-wall smart nanochannels", *Anal Chem*, **95**(2), pp. 1522–1531 (2023). https://doi.org/10.1021/acs.analchem.2c04559
44. Khatibi, M., Ashrafizadeh, S.N., and Sadeghi, A. "Augmentation of the reverse electrodialysis power generation in soft nanochannels via tailoring the soft layer properties", *Electrochim Acta*, **395**, p. 139221 (2021). https://doi.org/10.1016/j.electacta.2021.139221
45. Ayoubi, S., Khatibi, M., and Ashrafizadeh, S.N. "A variational approach applied to reduce fouling with the electroosmotic flow in porous-wall microchannels", *Microfluid Nanofluidics*, **25**(12), p. 101 (2021). https://doi.org/10.1007/s10404-021-02501-3
46. Karimzadeh, M., Khatibi, M., and Ashrafizadeh, S.N. "Impacts of the temperature-dependent properties on ion transport behavior in soft nanochannels", *International Communications in Heat and Mass Transfer*, **129**, p. 105728 (2021). https://doi.org/10.1016/j.icheatmasstransfer.2021.105728
47. Ganjizade, A., Sadeghi, A., and Ashrafizadeh, S.N. "Effect of ion partitioning on electrostatics of soft particles with volumetrically charged inner core coated with pH-regulated polyelectrolyte layer", *Colloids Surf B Biointerfaces*, **170**, pp. 129–135 (2018). https://doi.org/10.1016/j.colsurfb.2018.05.053
48. Ganjizade, A., Ashrafizadeh, S.N., and Sadeghi, A. "Effect of ion partitioning on electrophoresis of soft particles", *Colloid Polym Sci*, **297**(2), pp. 191–200 (2019). https://doi.org/10.1007/s00396-018-04467-1
49. Seifollahi, Z. and Ashrafizadeh, S.N. "Ionic-size dependent electroosmotic flow in ion-selective biomimetic nanochannels", *Colloids Surf B Biointerfaces*, **216**, p. 112545 (2022). https://doi.org/10.1016/j.colsurfb.2022.112545
50. Seifollahi, Z. and Ashrafizadeh, S.N. "Effect of charge density distribution of polyelectrolyte layer on electroosmotic flow and ion selectivity in a conical soft nanochannel", *Chem Eng Sci*, **261**, p. 117986 (2022). https://doi.org/10.1016/j.ces.2022.117986
51. Li, X. Bin, Li, F.C., Yang, J.C., Kinoshita, et al. "Study on the mechanism of droplet formation in T-junction microchannel", *Chem Eng Sci*, **69**(1), pp. 340–351 (2012). https://doi.org/10.1016/j.ces.2011.10.048

Biographies

Farshad Raji received his BSc degree from the Univ. of Hakim Sabzevari at sabzevar Iran on 2018. Then he graduated with an MSc degree from the University of Iran university of science and technology, Iran on 2020. Currently, he is a PhD student at the Chemical and Petroleum Engineering Department at Sharif University. His current research interests include; microfluidics, adsorption, removal of pollution, and water treatment.

Mohammad Kazemeini received his BSc degree from the University of Minnesota at Minneapolis USA on 1984. Then he graduated with an MSc degree from the University of Virginia at Charlottesville, USA on 1986. Finally, he received his PhD degree from the University of Illinois at Chicago, USA on 1990. Currently, he is a faculty member at the Chemical and Petroleum Engineering Department at the Sharif University holding a distinguished Professor Rank. His current research interests include; preparation, characterization and physiochemical evaluations as well as; mathematical modelling of chemical and physical kinetics of regular, Core-Shell and Magnetic catalysts. Furthermore, investigating Alumina, carbons (CNTs, Graphene Oxide and carbon Nano-Fibers), Zeolites and MOF supported catalysts and sorbents are being worked on. Moreover, designing and fabrication as well as investigating performance of microreactors and microfluidic systems applied to catalytic HDS and ODS (i.e.; Hydro- and Oxidative- Desulfurization) as well as; photocatalytic and catalytic API (i.e.; activated pharmaceutical ingredients) and organic as well as pharmaceutical pollutants removing materials are of close and recent interests.